ACS APPLIED MATERIALS & INTERFACES

Research Article

www.acsami.org

Atomic Layer Deposition Encapsulated Activated Carbon Electrodes for High Voltage Stable Supercapacitors

Kijoo Hong,[†,‡] Moonkyu Cho,[‡] and Sang Ouk Kim*[,†]

[†]Department of Materials Science and Engineering, KAIST, Center for Nanomaterials and Chemical Reactions, Institute for Basic Science (IBS), Daejeon 305-701, Republic of Korea

[‡]Advanced Battery Materials Research Center, GS Energy Corporation, Seoul 134-848, Republic of Korea

Supporting Information

ABSTRACT: Operating voltage enhancement is an effective route for high energy density supercapacitors. Unfortunately, widely used activated carbon electrode generally suffers from poor electrochemical stability over 2.5 V. Here we present atomic layer deposition (ALD) encapsulation of activated carbons for high voltage stable supercapacitors. Two-nanometer-thick Al_2O_3 dielectric layers are conformally coated at activated carbon surface by ALD, well-maintaining microporous morphology. Resultant electrodes exhibit excellent stability at 3 V operation with 39% energy density enhancement from 2.5 V operation. Because of the protection of surface functional groups and reduction of electrolyte degradation, 74% of initial voltage was maintained 50 h after full charge, and 88% of capacitance was retained after 5000 cycles at 70 °C accelerated test, which correspond to 31 and 17% improvements from bare activated carbon, respectively. This ALD-based surface modification offers a general method to enhance electrochemical stability of carbon materials for diverse energy and environmental applications.

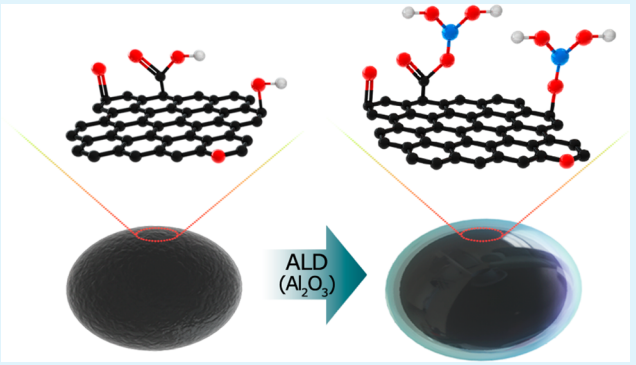

KEYWORDS: *atomic layer deposition, supercapacitor, electrode, activated carbon, encapsulation*

INTRODUCTION

A supercapacitor is a typical high power energy storage device, widely exploited for portable electronics, electric vehicles and so on.[1−3] Because electrical energy is restored by charge separation in a Helmholtz double layer,[4−10] electrode material is the crucial element to govern the ultimate performance of supercapacitors. Presently, supercapacitor electrodes principally rely upon activated carbons with large surface area, good electrochemical stability, and low cost.[3,4,9,10] Unfortunately, activated carbon electrodes commonly suffer from high leakage current, which results in self-discharge and low efficiency charging/discharging cycles with a significant amount of energy waste.[11−15] Because leakage current increases exponentially with applied voltage,[11,16] how to minimize leakage current is a critical issue for high performance supercapacitor particularly operating at high voltages.

Currently, fully charged voltage of single-cell commercial supercapacitor typically ranges from 2.5 to 2.7 V. Since specific energy of carbon/carbon capacitor scales with the square of fully charged voltage, enhancement of operating voltage is a facile route for large energy density.[7,17] It is possible to increase the operating voltage over 2.7 V by differentiating the relative masses of the two electrodes.[18−21] However, such an asymmetric design inevitably sacrifices charge capacitance. By contrast, in a symmetric design, the capacitance fading for cycle occurs rapidly under a high operating voltage over 2.5 V. This is principally due to the decomposition of the electrolyte at electrode surface, which can be further accelerated in the presence of surface functional groups.[5,22−26]

In this work, we introduce high-voltage-stable, high-performance activated carbon electrodes encapsulated with ultrathin Al_2O_3 dielectric layer by atomic layer deposition (ALD). ALD is a unique process that enables conformal coating of ultrathin layers at three-dimensional structures with atomic scale thickness controllability.[27−34] Our ALD-assisted process is free from the time-consuming thermal annealing process and thereby remarkably reduces processing time for carbon activation process. Activated carbon encapsulated with ultrathin Al_2O_3 layer demonstrates excellent electrochemical stability and exhibits remarkably performance enhancements in energy density (46 Wh kg^{-1}) as well as power (86 kW kg^{-1}) at 3 V operation (33 Wh kg^{-1}, 60 kW kg^{-1} at 2.5 V operation). These results are among the most advanced values reported thus far for the supercapacitor based on typical activated carbon electrodes.[35−47]

Received: November 3, 2014
Accepted: December 30, 2014
Published: December 30, 2014

DOI: 10.1021/am507673j
ACS Appl. Mater. Interfaces 2015, 7, 1899−1906

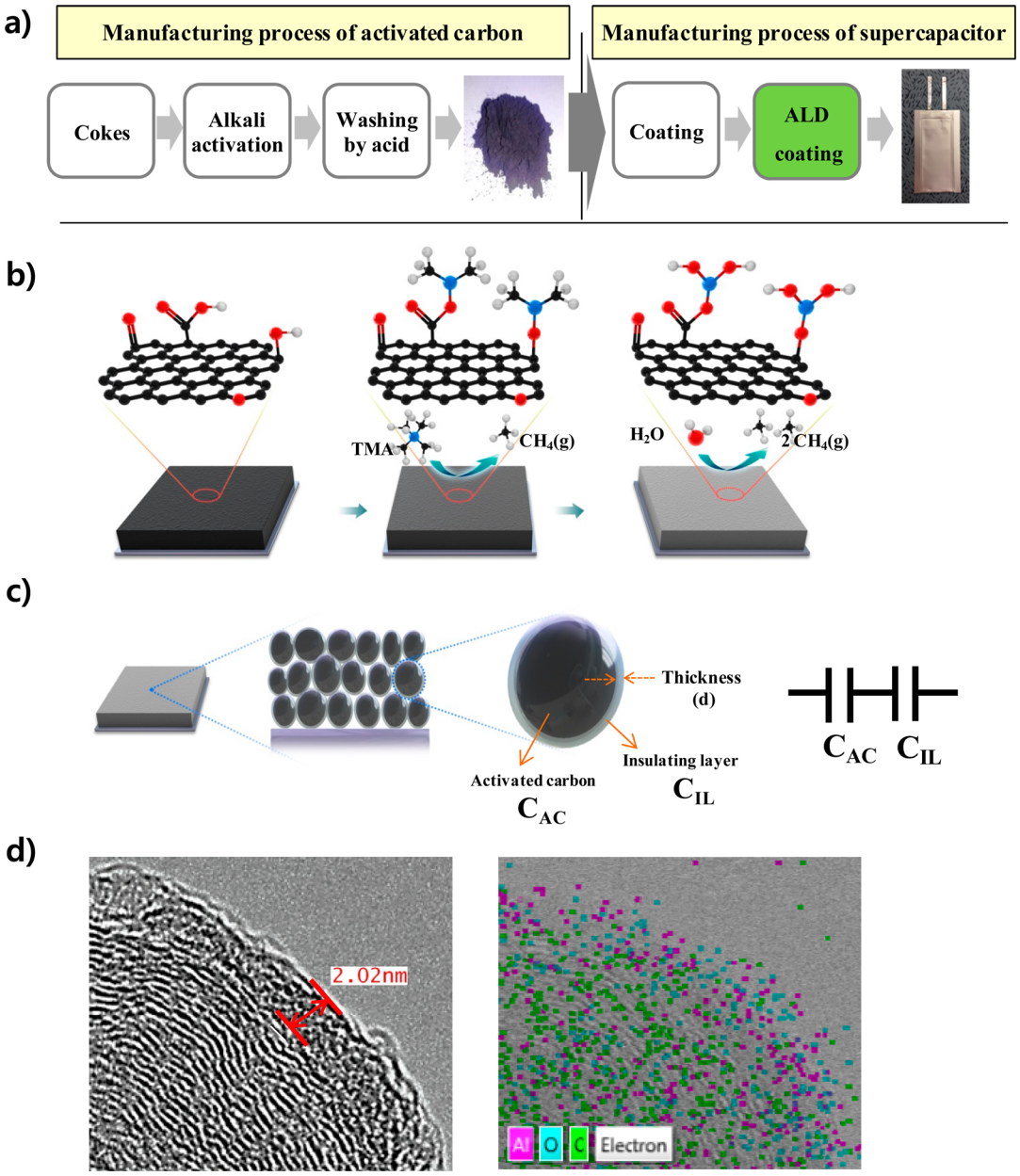

Figure 1. (a) Fabrication procedure for supercapacitor based on Al_2O_3 deposited activated carbon. (b) Schematic illustration of chemical reaction for Al_2O_3 ALD on activated carbon. (c) Schematic illustration, (d) HRTEM and mapping image of activated carbon with ALD Al_2O_3 layer.

RESULTS AND DISCUSSIONS

Our procedure for supercapacitor fabrication is briefly described in Figure 1a. In contrast to the conventional carbon activation process (see Figure S1a in the Supporting Information), thermal annealing and vacuum drying steps are replaced with ALD process. This simplification is advantageous for low production cost with minimum time delay (from 24 h to 10 min). Figure 1b schematically illustrates ALD process of ultrathin Al_2O_3 layer. Trimethylaluminum (TMA) and H_2O precursors are alternately supplied for controlled Al_2O_3 deposition. First, TMA is exposed on activated carbon surface with dense functional groups formed by acid washing. TMA molecules react with the hydroxyl groups to form C−O−Al $(CH_3)_2$ species. Following release of H_2O causes the reaction between H_2O and $AlCH_3$ to yield Al−OH species. It is noteworthy that the surface functional groups, such as hydroxyl groups, induced by acid washing can be straightforwardly employed for the reactive sites for ALD process. Furthermore, thermal annealing indispensably following the acid washing process in the traditional active carbon process can be excluded.

Figure 1c illustrates our Al_2O_3 deposited activated carbon. The capacitance of activated carbon (C_{AC}) is connected to the capacitance of insulating layer (C_{IL}) in a serial way. The equivalent capacitance of activated carbon with insulating layer is represented as $C_{eq} = C_{AC}C_{IL}/(C_{AC} + C_{IL})$ [C_{AC}, capacitance for activated carbon; C_{IL}, capacitance for insulating layer], which is always smaller than C_{AC}. Therefore, C_{IL} must be much larger than C_{AC} in order to not to sacrifice the overall capacitance. Because of the very small distance (d) at $C = \varepsilon_r\varepsilon_0 A/d$, this is possible if a high dielectric material is applied as an insulating layer.[39]

High-resolution transmission electron microscope (HRTEM) and elemental mapping were performed to investigate the structural and chemical modification of

DOI: 10.1021/am507673j
ACS Appl. Mater. Interfaces 2015, 7, 1899−1906

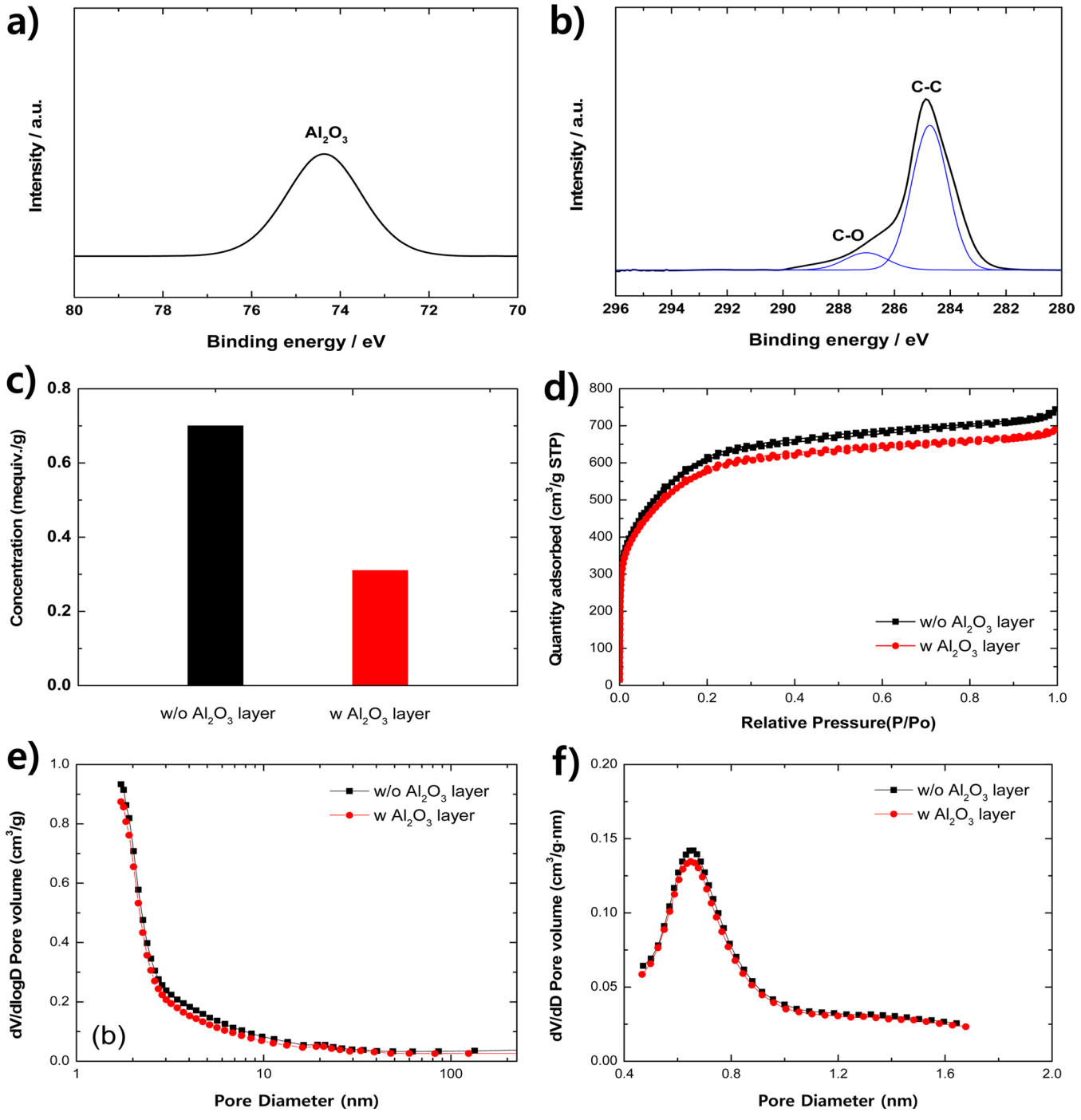

Figure 2. (a) XPS Al 2p spectrum, (b) XPS C 1s spectrum of activated carbon with ALD Al_2O_3 layer. (c) Boëhm titration. (d) Ar gas adsorption/desorption isotherm. Pore size distribution for Ar by using (e) BJH method and (f) HK method.

activation carbon after ALD coating, as shown in Figures 1d. The surface of activated carbon was well-encapsulated with ultrathin amorphous layer with 2 nm thickness. Elemental mapping confirmed the existence of Al and O elements. Notably, conformal encapsulation with ultrathin Al_2O_3 layer did not cause any significant structural change in bulk morphology. As demonstrated in Figure 1b, the thickness of Al_2O_3 layer was controllable by the cycle number of ALD (see Figure S2 in the Supporting Information). A 2 nm thickness is chosen to avoid any capacitance reduction, as mentioned above.

We employed X-ray photoelectron spectroscopy (XPS) for the detailed chemical structure characterization. In Al 2p spectrum (Figure 2a), the peak at 74.3 eV is assigned to the formation of Al_2O_3 at surface of activated carbon. Deconvoluted C 1s XPS spectrum shows the two peaks around 285.3 and 287 eV, the former of which is assigned to the C−C bonding in disordered carbon. The peak at 287 eV corresponds to hydroxyl (C−OH) groups. In contrast to the XPS C 1s spectrum for activated carbon without Al_2O_3 layer (see Figure S3b in the Supporting Information), the peak intensities for oxygen function groups (C−OH at 287 eV, OH-C═O at 289 eV) decreased significantly. Table 1 summarizes the relative intensities normalized with C−C bond intensity. Obviously, Al_2O_3 layer substituted a lot of oxygen functional groups at the

DOI: 10.1021/am507673j
ACS Appl. Mater. Interfaces 2015, 7, 1899−1906

Table 1. Comparison of Chemical and Physical Properties of Activated Carbon with or without ALD Al_2O_3 Layer

analysis	item	w Al_2O_3 layer	w/o Al_2O_3 layer
XPS[a]	C−C (285.3 eV)	100	100
	C═O (287.0 eV)	14.8	29
	COOH (289.0 eV)		8.9
Boëhm titration	concentration (mequiv./g)	0.31	0.70
BET & BJH (Ar gas)	surface area (m^2 g^{-1})	1900	1850
	pore volume (cm^3 g^{-1})	0.9	0.86
	average Pore width (nm)	2	2
HK (Ar gas)	median pore width (nm)	0.8	0.8

[a]Relative intensity of each bond in XPS analysis of C 1s spectra.

surface of activated carbon.[23−26] Quantitative analysis of acidic oxygen functional groups by Boëhm titration[23] (Figure 2c) revealed that the concentration of surface groups after ALD was 0.31 mequiv g^{-1}, which is less than the half of bare activated carbon.

The surface area of ALD modified activated carbon was measured by N_2 (77.4 K) and Ar (87.3 K) adsorption/desorption. Bare activated carbon without Al_2O_3 layer was measured as a reference. As shown in Figure 2d, Ar isotherm presents the type I isotherm curve, which is typical for microporous solids. N_2 isotherm also showed an identical feature (see Figure S3c in the Supporting Information). Notably, ALD coating does not decrease surface area and pore volume significantly (from 1900 m^2 g^{-1} and 0.9 cm^3 g^{-1} to 1850 m^2 g^{-1} and 0.86 cm^3 g^{-1}) (Table 2). Notably, such a

Table 2. Cell Thickness and Impedance Change after 5000th Cycle for Pouch Cell

	cycle no.	w Al_2O_3 layer	w/o Al_2O_3 layer
cell thickness (mm)	1st	0.5	0.5
	5000th	0.52	3.22
swelling rate (%)		4	644
cell impedance (Ω cm^2)	1st	0.92	0.53
	5000th	1.05	1.84
increase (%)		14	347

minor change is also due to high density of Al_2O_3 rather than pore-filling by Al_2O_3.[48] In addition, pore size distribution was obtained by using BJH (Barret−Joyner−Halenda) and HK (Horvath−Kawazoe) methods from the adsorption/desorption isotherms to clarify any pore blocking by ALD coating. The BJH shows that peak intensity of pore diameter of 2 nm decreased slightly but peak position was maintained the same value (Figure 2e and Figure S3d in the Supporting Information). The HK method available for micropore ($d \leq$ 2 nm) smaller than coating thickness did not detect any change in pore diameter after ALD coating (Figure 2f). Taken together, it is verified that highly conformal ALD Al_2O_3 layer does not block neither mesopore nor micropore channels of activated carbon.

Cyclic voltammogram (CV) in the extended potential range from 2.5 to 3.0 V (at 50 mV s^{-1} @ 70 °C) was employed to evaluate electrochemical stability (Figures 3a-c). ALD coated activated carbon not only retained rectangular shape without significant distortion but also showed large total charge storage capacity (Q_{tot}) values (Figure 3d). This is attributed to the significant role of ALD layer to prevent the side reaction of electrolyte, which may increase of resistance of electrode interface. Consequently, the Q_{tot} of ALD coated carbon continuously increased in a proportional way with charge potential, whereas the Q_{tot} of bare activated carbon showed a minor enhancement, which is principally limited by the IR drop arising from interfacial resistance.

The electrochemical reversibility was compared by the relative ratio of anodic and cathodic charge (Q_a/Q_c) (Figure 3d). ALD coated activated carbon shows highly reversible electrochemical process represented by a low ratio of Q_a/Q_c around 1.15. Surprisingly, almost constant Q_a/Q_c was maintained up to 3 V, indicating negligible irreversibility. By contrast, bare activated carbon revealed significant irreversibility, which becomes even more serious with potential increase. On the basis of these results, a stable operating potential region for ALD-coated carbon could be extended up to 3 V.

The electrochemical properties of supercapacitor were analyzed in a pouch type cell with two electrodes and 1.0 M tetraethylammonium tetrafluoroborate (Et_4NBF_4) in acetonitrile electrolyte. We chose large pouch cell rather than coin cell to evaluate electrochemical properties under real application conditions, as shown in Figure S1b in the Supporting Information (electrode dimension: 30 × 42 mm, cell capacitance: 1 F). Particularly, charge voltages from 2.7 to 3.0 V were examined to assess high voltage stability, as suggested from CV results. The specific capacitance was evaluated by galvanostatic charge−discharge test shown in Figure 4a. The linear voltage−time curves exhibited a good capacitive behavior without any irreversible reaction. The specific capacitance was calculated by the equation $C_{sc} = I(T_2 - T_1)/[(V_1 - V_2)m]$, where V_1 and V_2 represent $V_{max}0.8$ and $V_{max}0.4$ V, respectively (based on IEC62391−1), I = 0.5 A g^{-1} and m is the weight of the two electrodes. The specific capacitance of supercapacitor with ALD-coated activated carbon was 37 F g^{-1}, which is almost same with that of activated carbon (38 F g^{-1}) (Figure 4a). This again confirms that porous structure was well-maintained without pore blocking during ALD coating. Further operation at a higher voltage significantly improved the energy density. Typically, while fully charged voltage increased to 3.0 V, energy density increased by at least 30% compared to 2.7 V operation.

Our activated carbon with significantly reduced functional groups at high surface area shows remarkable improvement for leakage current, which has remained as one of the most difficult technological problems for high performance supercapacitors. Self-discharge profile was examined in order to characterize any leakage current. After the supercapacitor was charged with a constant-voltage supply for 1 h, the open circuit voltage at the cell terminals was monitored for 50 h, as shown in Figure 4b. Surprisingly, even though 50 h passed after full charge to 3.0 V, it still retains 2.21 V (74% of initial voltage). By contrast, bare activated carbon showed 1.69 V (56% of initial voltage).

The principal source of self-discharge is faradic reactions at the electrode surface, as mentioned above. The surface oxygen functional groups (i.e., COOH, C═O, COOR, C−OH) behave as active sites for electrochemical oxidation/reduction, when electrodes were excessively polarized in an anodic or cathodic direction in the electrolytic solution. As a majority of functional groups at activated carbon were replaced with the Al_2O_3 layer, faradaic reaction between the electrode and electrolyte can be greatly reduced. So far, only a few studies have investigated on the reduction of leakage current, still along

DOI: 10.1021/am507673j
ACS Appl. Mater. Interfaces 2015, 7, 1899−1906

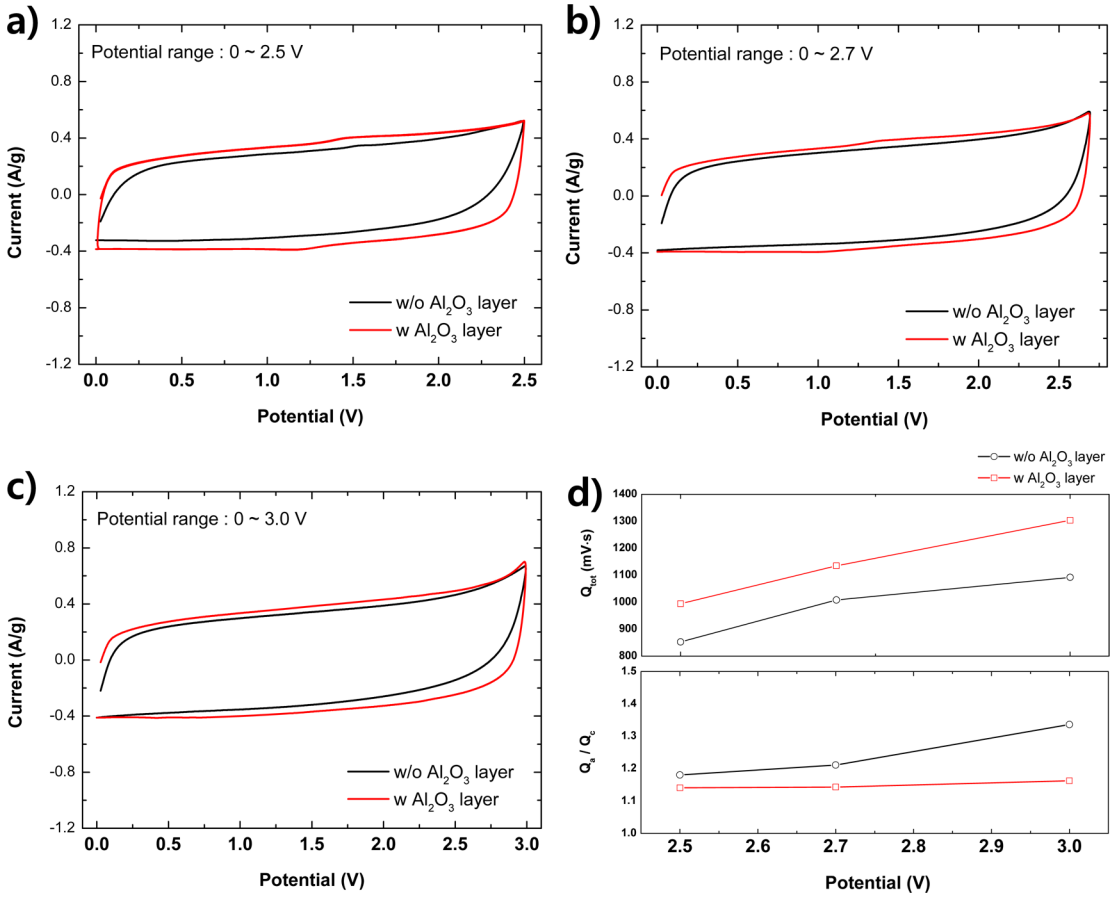

Figure 3. (a–c) Cyclic voltammograms, (d) total charge (Q_{tot}) and the ratio of anodic to cathodic charge (Q_a/Q_c) according to potential range change at 50 mV s^{-1}@70 °C.

with severe side effects such as capacitance reduction.[39] By contrast, our approach works even better for reducing leakage under high voltages over 3 V.

Another crucial requirement for high voltage stability is the cycle-ability at high voltage operation. In this work, supercapacitors were fully charged-discharged from 0 to 3.0 V for 5 K cycles at 70 °C. In such an accelerated cycle test at a high temperature, Arrhenius model is generally used to extrapolate the temperature dependence of life (rate of a chemical reaction $K = A \exp(-E_a/RT)$, where A, E_a, R, and T are the constant, activation energy, gas constant, and temperature in Kelvin, respectively).[16,49,50] It is commonly regarded that the cycle life is halved for every 10 °C increase. On the basis of this assumption, we can regard that 5 K cycles at 70 °C can be converted into 120 K cycles at room temperature. Notably, supercapacitors based on our ALD coated activated carbon exhibited excellent stability despite the extreme test condition (Figure 4c). After 5 K constant current charge/discharge cycles at current density of 1 A g^{-1}, 88% of its initial capacitance was retained. By contrast, the supercapacitors based on bare activated carbon declined down to 75% along with a rapid decay within 200 cycles. Furthermore, the swelling phenomenon of supercapacitors in high voltages causes severe problems such as leakage, pollution, and breakdown. Practically, supercapacitors based on bare activated carbon were swollen extremely (Figure 4c inset, Table 2), some of which indeed show electrolyte leakage and breakdown. By contrast, supercapacitors with protective ALD coating layer well-preserved original dimension without any swelling, verifying that the surface of activated carbon was perfectly protected against side effects from electrolyte.

Electrochemical impedance spectroscopy (EIS) analysis has been recognized as one of the principal characterization methods for supercapacitors.[10,50−52] Impedance of both bare and ALD coated samples were measured after first and 5000th cycles in the frequency range of 500 kHz −5 MHz (Figure 4d, Table 2). At high frequencies, the intercept at real part (Re) is a combinational resistance of ionic resistance of electrolyte, intrinsic resistance of substrate and contact resistance at the active material/current collector interface. This value is almost same for both samples. A major difference was the semicircle in the high-frequency range shown in the inset, which corresponds to the charge-transfer resistance (R_{ct}). The R_{ct} is generated mainly from the charge transfer at the contact interface between the electrode and electrolyte. It can be calculated from the diameter of semicircle and geometric area of the electrodes (12.6 cm^2). After the first cycle, a resistance of 0.92 Ω cm^2 was calculated, which is larger than 0.53 Ω cm^2 for supercapacitor based on bare activated carbon (see Figure S4c in the Supporting Information). This is attributed to the resistance of Al_2O_3 layer. After 5 K cycles (Figure 4d), R_{ct} was measured to be 1.05 Ω cm^2 for ALD coated electrodes, which is almost same with initial value. By contrast, R_{ct} for bare activated carbon was significantly increased up to 1.84 Ω cm^2. Undesired reaction involved with electrolyte degradation occurred in such a rapid way without any protective layer.

The chemical structure of electrode after 5 K cycles was characterized by XPS. Typical elements for the byproduct

DOI: 10.1021/am507673j
ACS Appl. Mater. Interfaces 2015, 7, 1899−1906

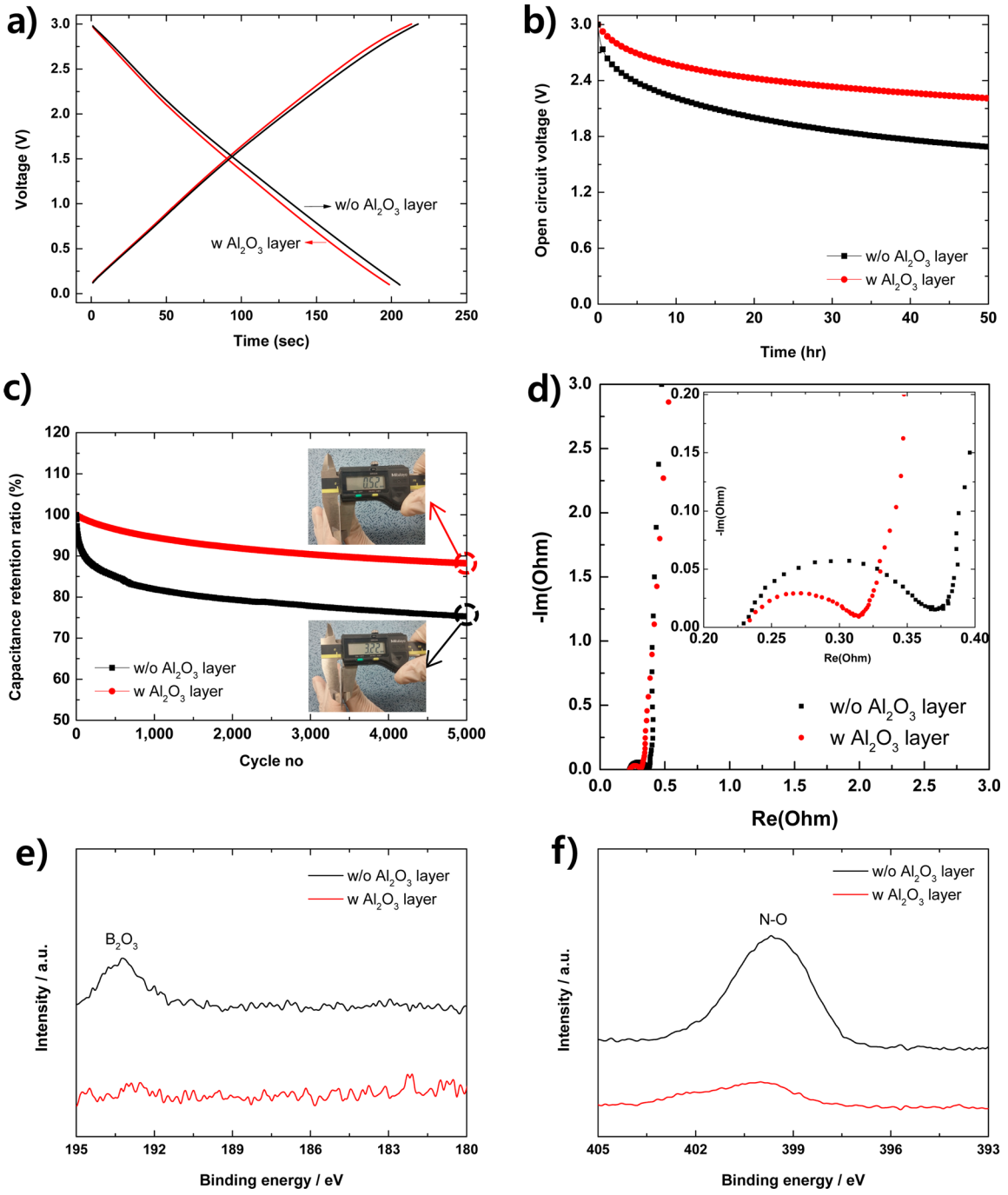

Figure 4. (a) Galvanostatic charge−discharge curves. (b) Self-discharge for 50 h. (c) Capacity retention during 5000 cycles at 70 °C. (insets) Thickness after 5 K cycles. (d) Electrochemical impedance spectrum after 5000 cycles. Inset shows magnified view at low-frequency range. (e) XPS B 1s spectrum, (f) XPS N 1s spectrum of cycled electrode. (voltage range; 0.1−3.0 V, current; 1 A g^{-1}).

generated from the decomposition of Et_4N^+ and BF_4^- ions are B and N, respectively. XPS B 1s and N 1s spectra are shown in Figure 4e, f. The surface density of B and N were observed much less at the surface of ALD coated activated carbon. The peak intensity of N is approximately one-third of that for bare carbon electrodes, whereas B was hardly detected at all. These results indicated that Al_2O_3 layer indeed offers a protective interface between electrode and electrolyte, which can indeed avoid the unnecessary decomposition of electrolytes.

CONCLUSIONS

We have demonstrated ultrathin 2 nm-thick Al_2O_3 encapsulation of activated carbon by ALD for ultrahigh performance supercapacitor with remarkable stability at high operating voltages. Although ALD encapsulation well-maintains the meso- and microporous structure of activated carbon without filling accessible pore channels, it greatly reduces the processing time for electrode fabrication by eliminating time-consuming thermal annealing and vacuum drying process. Significantly, ALD deposited Al_2O_3 layer effectively protected oxygen functional groups that cause faradaic degenerative reaction of

DOI: 10.1021/am507673j
ACS Appl. Mater. Interfaces 2015, 7, 1899−1906

electrolytes. Consequently, carbon electrodes were protected from undesirable reactions involved with electrolytes and exhibited excellent retention for charge/discharge cycles. This ALD-assisted stabilization is a general solution to the low-energy-density problem of activated-carbon-based supercapacitors. The resultant supercapacitor attains not only high power but also high energy density for more diversified applications.

MATERIALS AND METHODS

Synthesis of Activated Carbon. Coke (JX NOE) was first mixed with KOH powder mechanically (weight ratio of cokes to KOH is 1 to 4). For alkali activation, the Coke/KOH mixture was put in a tubular furnace under flowing N_2 and annealed at 750 °C for 1 h. Then heat-treated powder was washed with the mixture with diluted HCl and water subsequently, followed by a drying step to obtain activated carbon (but, in conventional method, annealing step has to be repeated again at a temperature higher than activation temperature after drying step, see Figure S1a in the Supporting Information).

Fabrication of Electrode. The electrode was prepared by casting slurries containing 80 wt % of AC, 10 wt % of acetylene black, 10 wt % of SBR/PTFE/CMC mixed in deionized water on Al foil (20 μm thickness); however, in the conventional method, it is necessary that the electrode was dried under vacuum over 24 h at 120 °C.

Atomic Layer Deposition. Al_2O_3 ALD layers were grown directly on activated carbon powders using a reactor. The tetramethylaluminum (TMA, EG chem.) and high performance liquid chromatography grade H_2O (HPLC, Sigma-Aldrich) were used as precursor. The typical growth rate for the chemistry is 1.1 Å per cycle. The reaction sequence was: (i) exposure of TMA, (ii) purge to remove the nonreacted precursors and the byproducts, (iii) exposure of H_2O, (iv) purge to remove the nonreacted precursors and the byproducts. ALD was conducted at 180 °C.

Electrochemical Measurements. The pouch-type cells were assembled to evaluate the electrochemical performances (see Figure S1b in the Supporting Information). One pair of cathode/anode electrodes with the dimension of 30 × 42 mm were stacked in a cell which was designed as two electrode system using 1.0 M tetraethylammonium tetrafluoroborate (Et_4NBF_4) in acetonitrile as an electrolyte. The galvanostatic charge/discharge measurements were carried out in the voltage range of 0–3.0 V on battery cycler (PNE solution, Korea). The electrochemical impedance spectrum was measured by a VMP3 instrument (Biologic Inc.).

The energy density, E (Wh kg^{-1}) was estimated as $E = CV^2/2$ (Ws/g) × 1000 (g/kg) × 1/3600 (h/s), where C is capacitance of the electrode, V is the operating voltage. The power density, P(W/kg) was calculated by diving energy density by the discharge time at different densities.

CHARACTERIZATION

The surface morphologies and microstructures were characterized by high-resolution transmission electron microscope (HRTEM, JEOL JEM-2100F). The chemical functional groups and byproducts on the surfaces were characterized by X-ray photoelectron spectroscopy (XPS, Thermo Scientific Sigma Probe) and Boëhm titration. The specific surface area, pore volume, and pore size distribution were obtained from Ar adsorption/desorption (Micrometrics, ASAP 2020).

ASSOCIATED CONTENT

Supporting Information

The photograph and schematic diagram of test cell, TEM · XPS · Boëhm data for bare activated carbon, N_2 adsorption/desorption analysis, and electrochemical data in the voltage range of 0–2.7 V. This material is available free of charge via the Internet at http://pubs.acs.org.

AUTHOR INFORMATION

Corresponding Author

*E-mail: sangouk.kim@kaist.ac.kr. Phone: +82-42-350-3339. Fax: +82-42-350-3310.

Notes

The authors declare no competing financial interest.

ACKNOWLEDGMENTS

This work was financially supported by Institute for Basic Science (IBS).

REFERENCES

(1) Armaroli, N.; Balzani, V. Towards an Electricity-Powered World. *Energy Environ. Sci.* **2011**, *4*, 3193–3222.
(2) Choi, B. G.; Yang, M.; Hong, W. H.; Choi, J. W.; Huh, Y. S. 3d Macroporous Graphene Frameworks for Supercapacitors with High Energy and Power Densities. *ACS Nano* **2012**, *6*, 4020–4028.
(3) Liu, C.; Li, F.; Ma, L. P.; Cheng, H. M. Advanced Materials for Energy Storage. *Adv. Mater.* **2010**, *22*, E28–E62.
(4) R. Miller, J.; Simon, P. Electrochemical Capacitors for Energy Management. *Science* **2008**, *321*, 651–652.
(5) Maiti, U. N.; Lim, J. W.; Lee, K. E.; Lee, W. J.; Kim, S. O. Three-Dimensional Shape Engineered, Interfacial Gelation of Reduced Graphene Oxide for High Rate, Large Capacity Supercapacitors. *Adv. Mater.* **2013**, *26*, 615–619.
(6) Han, T. H.; Lee, W. J.; Lee, D. H.; Kim, J. E.; Choi, E. Y.; Kim, S. O. Peptide/Graphene Hybrid Assembly into Core/Shell Nanowires. *Adv. Mater.* **2010**, *22*, 2060–2064.
(7) Izadi-Najafabadi, A.; Yasuda, S.; Kobashi, K.; Yamada, T.; N.Futaba, D.; Hatori, H.; Yumura, M.; lijima, S.; Hata, K. Extracting the Full Potential of Single-Walled Carbon Nanotubes as Durable Supercapacitor Electrodes Operable at 4 V with High Power and Energy Density. *Adv. Energy Mater.* **2010**, *22*, E235–E241.
(8) Lee, J. H.; Park, N. K.; Kim, B. G.; Jung, D. S.; Im, K. H.; Hur, J. H.; Choi, J. W. Restacking-Inhibited 3D Reduced Graphene Oxide for High Performance Supercapacitor Electrodes. *ACS Nano* **2013**, *10*, 9366–9374.
(9) Hulicova-Jurcakova, D.; Seredych, M.; Lu, G. Q.; Bandosz, T. J. Combined Effect of Nitrogen- and Oxygen-Containing Functional Groups of Microporous Activated Carbon on Its Electrochemical Performance in Supercapacitors. *Adv. Funct. Mater.* **2009**, *19*, 438–447.
(10) Wei, L.; Sevilla, M.; Fuertes, A. B.; Mokaya, R.; Yushin, G. Polypyrrole-Derived Activated Carbons for High-Performance Electrical Double-Layer Capacitors with Ionic Liquid Electrolyte. *Adv. Funct. Mater.* **2012**, *22*, 827–834.
(11) Ricketts, B. W.; Ton-That, C. Self-Discharge of Carbon-Based Supercapacitors with Organic Electrolytes. *J. Power Sources* **2000**, *89*, 64–69.
(12) Gungor, V. C.; Hancke, G. P. Industrial Wireless Sensor Networks: Challenges, Design Principles, and Technical Approaches. *IEEE Trans. Ind. Electron.* **2009**, *56*, 4258–4265.
(13) M. Oickle, A.; A.Andreas, H. Examination of Water Electrolysis and Oxygen Reduction As Self-Discharge Mechanisms for Carbon-Based, Aqueous Electrolyte Electrochemical Capacitors. *J. Phys. Chem. C* **2011**, *115*, 4283–4288.
(14) Obreja, V. V. N. On the Performance of Supercapacitors with Electrodes Based on Carbon Nanotubes and Carbon Activated Material – A review. *Phys. E (Amsterdam, Neth.)* **2008**, *40*, 2596–2605.
(15) Yang, H.; Zhang, Y. Self-discharge Analysis and Characterization of Supercapacitors for Environmentally Powered Wireless Sensor Network Applications. *J. Power Sources* **2011**, *196*, 8866–8873.
(16) Uno, M.; Tanaka, K. Accelerated Charge-Discharge Cycling Test and Cycle Life Prediction Model for Supercapacitors in Alternative Battery Applications. *IEEE Trans. Ind. Electron.* **2012**, *59*, 4704–4712.

DOI: 10.1021/am507673j
ACS Appl. Mater. Interfaces 2015, 7, 1899–1906

(17) Grote, F.; Lei, Y. A Complete Three-Dimensionally Nanostructured Asymmetric Supercapacitor with High Operating Voltage Window Based on PPy and MnO_2. *Nano Energy* **2014**, *10*, 63−70.
(18) Zhang, J.; Jiang, J.; Li, H.; Zhao, X. S. A High-Performance Asymmetric Supercapacitor Fabricated with Grapheme-Based Electrodes. . *Energy Environ. Sci.* **2011**, *4*, 4009−4015.
(19) Cericola, D.; Kötz, R.; Wokaun, A. Effect of Electrode Mass Ratio on Aging of Activated Carbon Based Supercapacitors Utilizing Organic Electrolytes. *J. Power Sources* **2011**, *196*, 3114−3118.
(20) Yan, J.; Wang, Q.; Wei, T.; Fan, Z. Recent Advances in Design and Fabrication of Electrochemical Supercapacitors with High Energy Densities. *Adv. Mater.* **2014**, *4*, 1300816.
(21) Béguin, F.; Presser, V.; Balducci, A.; Frackowiak, E. Carbons and Electrolytes for Advanced Supercapacitors. *Adv. Mater.* **2014**, *26*, 2219−2251.
(22) Lai, L.; Yang, H.; Wang, L.; Teh, B. K.; Zhong, J.; Chou, H.; Chen, L.; Chen, W.; Shen, Z.; S. Ruoff, R.; Lin, J. Preparation of Supercapacitor Electrodes through Selection of Graphene Surface Functionalities. *ACS Nano* **2012**, *6*, 5941−5951.
(23) Azaïs, P.; Duclaux, L.; Florian, P.; Massiot, D.; Lillo-Rodenas, M.; Linares-Solano, A.; Peres, J.; Jehoulet, C.; Béguin, F. Causes of Supercapacitors Ageing in Organic Electrolyte. *J. Power Sources* **2007**, *171*, 1046−1053.
(24) Oda, H.; Yamashita, A.; Minoura, S.; Okamoto, M.; Morimoto, T. Modification of the Oxygen-Containing Functional Group on Activated Carbon Fiber in Electrodes of an Electric Double-Layer Capacitor. *J. Power Sources* **2006**, *158*, 1510−1516.
(25) Yoshida, A.; Tanahashi, I.; Nishino, A. Effect of Concentration of Surface Acidic Functional Groups on Electric Double-Layer Properties of Activated Carbon Fibers. *Carbon* **1990**, *28*, 611−615.
(26) Jansen, R. J. J.; Bekkum, H. V. XPS of Nitrogen-Containing Functional Groups on Activated Carbon. *Carbon* **1995**, *33*, 1021−1027.
(27) Meng, X.; Yang, X.; Sun, X. Emerging Applications of Atomic Layer Deposition for Lithium-Ion Battery Studies. *Adv. Mater.* **2012**, *24*, 3589−3615.
(28) Marichy, C.; Bechelany, M.; Pinna, N. Atomic Layer Deposition of Nanostructured Materials for Energy and Environmental Applications. *Adv. Mater.* **2012**, *24*, 1017−1032.
(29) Woo, J. H.; Trevey, J. E.; Cavanagh, A. S.; Choi, Y. S.; Kim, S. C.; George, S. M.; Oh, K. H.; Lee, S. H. Nanoscale Interface Modification of $LiCoO_2$ by Al_2O_3 Atomic Layer Deposition for Solid-State Li batteries. *J. Electrochem. Soc.* **2012**, *159*, A1120−A1124.
(30) Xiao, X.; Lu, P.; Ahn, D. J. Ultrathin Multifunctional Oxide Coatings for Lithium Ion Batteries. *Adv. Mater.* **2011**, *23*, 3911−3915.
(31) Jung, Y. S.; Cavanagh, A. S.; Riley, L. A.; Kang, S. H.; Dillon, A. C.; Groner, M. D.; George, S. M.; Lee, S. H. Ultrathin Direct Atomic Layer Deposition on Composite Electrodes for Highly Durable and Safe Li-Ion Batteries. *Adv. Mater.* **2010**, *22*, 2172−2176.
(32) Leskelä, M.; Ritala, M. Atomic Layer Deposition(ALD): from Precursors to Thin Film Structures. *Thin Solid Films* **2002**, *409*, 138−146.
(33) Dillon, A. C.; Ott, A. W.; Way, J. D.; George, S. M. Surface Chemistry of Al_2O_3 Deposition Using $Al(CH_3)_3$ and H_2O in a Binary Reaction Sequence. *Surf. Sci.* **1995**, *322*, 230−242.
(34) Moon, H. S.; Kim, J. Y.; Jin, H. M.; Lee, W. J.; Choi, H. J.; Mun, J. H.; Choi, Y. J.; Cha, S. K.; Kwon, S. H.; Kim, S. O. Atomic Layer Deposition Assisted Pattern Multiplication of Block Copolymer Lithography for 5nm Scale Nanopatterning. *Adv. Mater.* **2014**, *24*, 4343−4348.
(35) Sevilla, M.; Fuertes, A. B. Direct Synthesis of Highly Porous Interconnected Carbon Nanosheets and Their Applications as High-Performance Supercapacitors. *ACS Nano* **2014**, *8*, 5069−5078.
(36) Wen, Z.; Wang, X.; Mao, S.; Bo, Z.; Kim, H. J.; Cui, S.; Lu, G.; Feng, X.; Chen, J. Crumpled Nitrogen-Doped Graphene Nanosheets with Ultrahigh Pore Volume for High-performance Supercapacitor. *Adv. Mater.* **2012**, *24*, 5610−5616.
(37) Lu, W.; Hartman, R.; Qu, L.; Dai, L. Nanocomposite Electrodes for High-Performance Supercapacitors. *J. Phys. Chem. Lett.* **2011**, *2*, 655−660.
(38) Hu, C.; Qu, W.; Rajagopalan, R.; Randall, C. Factors Influencing High Voltage Performance of Coconut Char Derived Carbon Based Electrical Double Layer Capacitor Made Using Acetonitrile and Propylene Carbonate Based Electrolytes. *J. Power Sources* **2014**, *272*, 90−99.
(39) Tevi, T.; Yaghoubi, H.; Wang, J.; Takshi, A. Application of Poly (p-phenylene oxide) as Blocking Layer to Reduce Self-discharge in Supercapacitors. *J. Power Sources* **2013**, *241*, 589−596.
(40) Bhattacharjya, D.; Kim, M. S.; Bae, T. S.; Yu, J. S. High Performance Supercapacitor Prepared from Hollow Mesoporous Carbon Capsules with Hierarchical Nanoarchitecture. *J. Power Sources* **2013**, *244*, 799−805.
(41) Yu, H.; Wu, J.; Fan, L.; Hao, S.; Lin, J.; Huang, M. An Efficient Redox-mediated Organic Electrolyte for High-energy Supercapacitor. *J. Power Sources* **2014**, *248*, 1123−1126.
(42) Yang, X.; Zhang, L.; Zhang, F.; Zhang, T.; Huang, Y.; Chen, Y. A High-performance All-solid-state Supercapacitor with Graphene-doped Carbon Material Electrodes and a Graphene oxide-doped Ion Gel Electrolyte. *Carbon* **2014**, *72*, 381−386.
(43) Hu, J.; Kang, Z.; Li, F.; Huang, X. Graphene with Three-dimensional Architecture for High Performance Supercapacitor. *Carbon* **2014**, *67*, 221−229.
(44) Ma, C.; Li, Y.; Shi, J.; Song, Y.; Liu, L. High-performance Supercapacitor Electrodes Based on Porous Flexible Carbon Nanofiber Paper Treated by Surface Chemical Etching. *Chem. Eng. J.* **2014**, *249*, 216−225.
(45) Zhu, Y. W.; Murali, S.; Stoller, M. D.; Ganesh, K. J.; Cai, W. W.; Ferreira, P. J.; Pirkle, A.; Wallace, R. M.; Cychosz, K. A.; Thommes, M.; et al. Carbon-Based Supercapacitors Produced by Activation of Graphene. *Science* **2011**, *332*, 1537−1541.
(46) Lee, W. J.; Maiti, U. N.; Lee, J. M.; Lim, J. W.; Han, T. H.; Kim, S. O. Nitrogen-Doped Carbon Nanotubes and Graphene Composite Structures for Energy and Catalytic Applications. *Chem. Commun.* **2014**, *50*, 6818−6830.
(47) Maiti, U. N.; Lee, W. J.; Lee, J. M.; Oh, Y. T.; Kim, J. Y.; Kim, J. E.; Shim, J. W.; Han, T. H.; Kim, S. O. 25th Aninniversary Article: Chemically Modified/Doped Carbon Nanotubes & Graphene for Optimized Nanostructures & Nanodevices. *Adv. Mater.* **2014**, *26*, 40−67.
(48) Dong, X.; Shen, W.; Gu, J.; Xiong, L.; Zhu, Y.; Li, H.; Shi, J. MnO_2-Embedded-in-Mesoporous-Carbon-Wall Structure for Use as Electrochemical Capacitors. *J. Phys. Chem. B* **2006**, *110*, 6015−6019.
(49) Vellacheri, R.; Al-Haddad, A.; Zhao, H.; Wang, W.; Wang, C.; Lei, Y. High Performance Supercapacitor for Efficient Energy Storage under Extreme Environmental Temperatures. *Nano Energy* **2014**, *8*, 231−237.
(50) Kötz, R.; Hahn, M.; Gallay, R. Temperature Behavior and Impedance Fundamentals of Supercapacitors. *J. Power Sources* **2006**, *154*, 550−555.
(51) Yang, W.; Gao, Z.; Song, N.; Zhang, Y.; Yang, Y.; Wang, J. Synthesis of Hollow Polyaniline Nano-capsules and Their Supercapacitor Application. *J. Power Sources* **2014**, *272*, 915−921.
(52) Warsi, M. F.; Shakir, I.; Shahid, M.; Sarfraz, M.; Nadeem, M.; Gilani, A. Conformal coating of Cobalt-Nickel Layered Double Hydroxides Nanoflakes on Carbon Fibers for High-performance Electrochemical Energy Storage Supercapacitor Devices. *Electrochim. Acta* **2014**, *135*, 513−518.

DOI: 10.1021/am507673j
ACS Appl. Mater. Interfaces 2015, 7, 1899−1906